

A search for strong magnetic fields in massive and very massive stars in the Magellanic Clouds

S. Bagnulo¹, G. A. Wade², Y. Nazé^{3,*}, J. H. Grunhut⁴, M. E. Shultz⁵, D. J. Asher¹, P. A. Crowther⁶, C. J. Evans⁷, A. David-Uraz⁵, I. D. Howarth⁸, N. Morrell⁹, M. S. Munoz¹⁰, C. Neiner¹¹, J. Puls¹², M. K. Szymański¹³, and J. S. Vink¹

¹ Armagh Observatory and Planetarium, College Hill, Armagh BT61 9DG, UK
e-mail: stefano.bagnulo@armagh.ac.uk

² Department of Physics and Space Science, Royal Military College of Canada, PO Box 17000, Station Forces, ON K7K 4B4, Canada

³ Institut d'Astrophysique et de Géophysique, Université de Liège, Quartier Agora (B5c), Allée du 6 Août 19c, 4000 Sart Tilman, Liège, Belgium

⁴ European Southern Observatory, Karl-Schwarzschild-Str. 2, 85748 Garching, Germany

⁵ Department of Physics and Astronomy, University of Delaware, Newark, DE 19716, USA

⁶ Department of Physics and Astronomy, University of Sheffield, Hicks Building, Hounsfield Road, Sheffield S3 7RH, UK

⁷ UK Astronomy Technology Centre, Royal Observatory, Blackford Hill, Edinburgh EH9 3HJ, UK

⁸ Department of Physics and Astronomy, University College London, Gower Street, London WC1E 6BT, UK

⁹ Las Campanas Observatory, Carnegie Observatories, Casilla 601, La Serena, Chile

¹⁰ Department of Physics, Engineering Physics and Astronomy, Queen's University, 64 Bader lane, Kingston, ON K7L 3N6, Canada

¹¹ LESIA, Paris Observatory, PSL University, CNRS, Sorbonne Université, Université de Paris, 5 place Jules Janssen, 92195 Meudon, France

¹² LMU München, Universitätssternwarte, Scheinerstr. 1, 81679 München, Germany

¹³ Astronomical Observatory, University of Warsaw, Aleje Ujazdowskie 4, 00-478 Warszawa, Poland

Received 11 November 2019 / Accepted 18 February 2020

ABSTRACT

Despite their rarity, massive stars dominate the ecology of galaxies via their strong, radiatively-driven winds throughout their lives and as supernovae in their deaths. However, their evolution and subsequent impact on their environment can be significantly affected by the presence of a magnetic field. While recent studies indicate that about 7% of OB stars in the Milky Way host strong, stable, organised (fossil) magnetic fields at their surfaces, little is known about the fields of very massive stars, nor the magnetic properties of stars outside our Galaxy. We aim to continue searching for strong magnetic fields in a diverse set of massive and very massive stars (VMS) in the Large and Small Magellanic Clouds (LMC/SMC), and we evaluate the overall capability of FORS2 to usefully search for and detect stellar magnetic fields in extra-galactic environments. We have obtained FORS2 spectropolarimetry of a sample of 41 stars, which principally consist of spectral types B, O, Of/WN, WNh, and classical WR stars in the LMC and SMC. Four of our targets are Of?p stars; one of them was just recently discovered. Each spectrum was analysed to infer the longitudinal magnetic field. No magnetic fields were formally detected in our study, although Bayesian statistical considerations suggest that the Of?p star SMC 159-2 is magnetic with a dipolar field of the order of 2.4–4.4 kG. In addition, our first constraints of magnetic fields in VMS provide interesting insights into the formation of the most massive stars in the Universe.

Key words. stars: magnetic field – stars: early-type – stars: Wolf-Rayet – stars: massive

1. Introduction

Magnetic fields are found in a wide variety of stars across the Hertzsprung-Russell diagram and in two quite different flavours. In the Sun and essentially all other low-mass stars ($M \lesssim 1.5 M_{\odot}$), vigorous magnetic activity is ubiquitous and responsible for most of the observed variability, and it is also essential to their formation and evolution. The magnetic fields have a complex structure, which generally changes on a timescale of days, weeks, or months; additionally, they produce non-thermal phenomena, such as a hot corona, prominences, flares, and sunspots. The fields are generally believed to be generated by a dynamo, which is produced by a combination of the motions of the deep convective outer layer of the star, together with the Coriolis force due

to rapid rotation, so that their strength often increases with the star's rotational velocity (see, e.g. [Reiners 2012](#)).

Despite the fact that stars with $M > 1.5 M_{\odot}$ do not host a significant outer convective envelope, some 5–10% of these higher-mass stars host strong magnetic fields (e.g. [Donati & Landstreet 2009](#); [Grunhut et al. 2017](#); [Sikora et al. 2019a](#)). These fields have a much smoother morphology than in solar-type stars, that is, organised on a larger scale, and their structure and geometry do not change on the timescales that have been observed so far (up to several decades; see for instance [Oksala et al. 2012](#); [Shultz et al. 2018](#); [Sikora et al. 2019b](#)). They do not produce surface stellar activity, and their strength does not increase with increasing stellar rotation rate: in fact, due to magnetic braking, the slowest rotators generally have very strong fields (e.g. [Shultz et al. 2019](#)). The favoured hypothesis is that the fields are fossil

* FNRS senior research associate.

remnants of the Galactic field that accumulated and possibly enhanced during an early phase of their evolution (e.g. Mestel 2001; Moss 2001; Neiner et al. 2015a). A competing hypothesis put forward in recent years suggests that the magnetic fields in higher-mass stars are the result of either a stellar merger event or a binary mass-transfer event (e.g. Tutukov & Fedorova 2010; Schneider et al. 2019). The merger hypothesis (e.g. Ferrario et al. 2009; Braithwaite & Spruit 2004) is also proposed to account for the highly-magnetic white dwarfs (Tout et al. 2008). This scenario seems to be supported by the low incidence rate of magnetic massive stars in close binaries, but it is severely challenged by the detection of the doubly magnetic system ϵ Lup (Shultz et al. 2015); furthermore, a study of massive close binaries with past or ongoing interaction did not reveal a larger incidence rate of magnetism (Nazé et al. 2017).

Observations of magnetic fields rely on the analysis of the Zeeman effect on the Stokes profiles of spectral lines (mainly Stokes V), which can only be normally detected in the brightest or in the most strongly magnetic stars. In fact, all of our knowledge regarding stellar magnetic fields is based on observations of Galactic stars. Therefore, seeing how the magnetic field acts in different environments with different metallicity would help to understand how magnetic fields, in particular fossil fields, originate, evolve, and interact with the circumstellar environment.

In that respect, hot, massive stars ($M \gtrsim 8 M_{\odot}$) are especially interesting targets for two reasons. On the one hand, they are bright enough to be observed at a reasonably high signal-to-noise ratio (S/N) in the galaxies that are closest to ours. On the other hand, their role in the chemistry of the Universe is especially important. They comprise only a small fraction of the stellar population of galaxies, yet they contribute a disproportionate amount of energy, matter, and momentum into their host galaxies throughout their lives via their strong, radiatively-driven winds, and when they die as supernovae (e.g. Crowther et al. 2010).

Knowledge of the magnetic properties of Galactic O and B stars has advanced remarkably over the last decade, largely due to the Magnetism in Massive Stars (MiMeS; Wade et al. 2016) and B-Fields in OB stars (BOB; Fossati et al. 2015) projects. These large-scale surveys have established their statistical incidence in the Galaxy ($\sim 7\%$ of B- and O-type stars are magnetic; Grunhut et al. 2017), the basic characteristics of these fields (i.e. strong, stable, and organised; e.g. Shultz et al. 2018), and they have begun to explore the rotational and magnetic evolution of these populations (e.g. Shultz et al. 2019; Petit et al. 2019). Furthermore, we are able to observe and model the important dynamical effects of the magnetic field on their stellar wind (e.g. Grunhut et al. 2012; ud-Doula et al. 2013; Nazé et al. 2014), and we are able to model and measure the magnetic spindown (e.g. ud-Doula et al. 2009; Townsend et al. 2010). Recent theoretical studies (e.g. Meynet et al. 2011; Keszthelyi et al. 2017, 2019) have also established basic predictions regarding the impact of magnetic fields on the lifetime and internal processes of these stars and, in turn, their impact on the late stages of stellar evolution and the properties of their degenerate remnants (e.g. Petit et al. 2017; Georgy et al. 2017).

An obvious next step towards improving our knowledge on the formation and characteristics of these fields is their study in extra-galactic environments. In fact, candidate extra-galactic magnetic hot, massive stars have recently been identified: a sample of five Of?p stars in the Large Magellanic Cloud (LMC) and Small Magellanic Cloud (SMC). These targets exhibit the telltale spectral peculiarities of the Of?p class (Walborn 1972, 1973) of which all Galactic examples are known to host strong magnetic

fields (Grunhut et al. 2017). In particular, they exhibit the characteristic periodic photometric and spectral modulation expected of hot magnetic stars (Nazé et al. 2015; Walborn et al. 2015). The first attempts to detect magnetic fields in these targets were carried out by Bagnulo et al. (2017, hereafter referred to as Paper I) who obtained FORS2 circular spectropolarimetry of them. No magnetic fields were formally detected with longitudinal field uncertainties as small as 350 G. In Paper I, we conclude that the magnetic fields of Of?p stars in the Magellanic Clouds are probably not much stronger, on average, than those of similar stars in our Galaxy.

Systematic observing campaigns, such as MiMeS, have mainly targeted stars with masses $\lesssim 60 M_{\odot}$, and only a handful of observations exist for stars with higher masses. No measurements exist for the stars with $M \gtrsim 100 M_{\odot}$. These very massive stars (VMS) are objects that are more massive than normal O-type stars and are identified as WNh stars (or Of/WN) stars, which are Wolf-Rayet stars with hydrogen in their spectra, and are thought to still be in the core hydrogen burning main sequence phase. The formation of these stars has been speculated to be the result of stellar mergers, although they may also simply form by disc fragmentation (Krumholz 2015). It has also been speculated that stellar mergers may be responsible for the generation of fossil magnetic fields of canonical massive stars (Schneider et al. 2016), a scenario that is backed up by magnetohydrodynamic simulations (Schneider et al. 2019). If VMS formation is attributable to stellar merging, one might therefore expect to find strong dipolar magnetic fields in VMS.

Setting constraints on the strength of the magnetic fields in VMS would have far reaching consequences regarding the origin of strong, stable magnetic fields in higher-mass stars. For instance, a magnetic incidence fraction $\gtrsim 10\%$ among very massive stars would provide strong evidence for the merger hypothesis as the origin of magnetism in higher-mass stars. In addition, spectropolarimetric observations of VMS serve the purpose of testing current dynamo models as alternative origins of magnetism in massive stars. In particular, VMS represent the ideal population of stars to test the sub-surface convection models of Cantiello et al. (2009). As shown by Cantiello & Braithwaite (2011, see their Fig. 1), the surface field strength of the magnetic field that is generated via this process is strongest in stars with very high masses ($\gtrsim 120 M_{\odot}$), reaching a minimum strength of ~ 300 G. Furthermore, theoretical models presented by Yusuf et al. (2013) show that the core masses of these VMS approach over 90% of the total stellar mass. MHD simulations indicate that the core dynamo-driven fields of main sequence B-type stars should be exceptionally strong (Augustson et al. 2016). Since the cores of VMS are larger, closer to the surface, and more vigorously convective, their putative core magnetic fields may be more easily detectable than at the stellar surface of less massive stars.

The purpose of this study is to extend the investigation carried out in Paper I to a larger and more diverse sample of stars (notably including VMS), in order to revisit candidate magnetic stars and to establish a better understanding of the realistic prospects for the detection of magnetic fields in B- and O-type stars outside the Milky Way. In order to accomplish this goal, we have obtained FORS2 Stokes V observations of extra-galactic Of?p stars (some have been previously studied, in Paper I, and another that had never been observed with spectropolarimetry before), seven extra-galactic VMS (with $M \gtrsim 100 M_{\odot}$), as well as a heterogenous sample of 35 (extra-galactic) stars located within a radius of 2–3 arcmin from the main targets, which were observed simply to take advantage of the instrument’s multi-object capabilities.

This paper is organised as follows: in Sect. 2 we describe our observing strategy and summarise the technique for data reduction and magnetic field measurements, which are reported in Sect. 4. In Sect. 5 we apply some statistical considerations and derive range estimates (almost exclusively upper limits) for the dipolar field strengths of the magnetic poles of the observed stars, and we discuss the various classes of star that we have observed: Of?p stars (Sect. 5.1), main sequence and evolved OBA stars (Sect. 5.2), cool supergiants (Sect. 5.3), and WR stars (Sect. 5.4). Implications for magnetic wind confinement in the circumstellar environments of VMS are developed in Sect. 5.5. In Sect. 6 we present our conclusions.

2. Observations

To search for magnetic fields in our targets, we used the FORS2 instrument (Appenzeller & Rupprecht 1992; Appenzeller et al. 1998) on the ESO VLT. FORS2 is a multipurpose instrument that is capable of imaging and low resolution spectroscopy, and it is equipped with polarimetric optics (a retarder waveplate and a Wollaston prism). Our observations were obtained in the context of two observing programs, one aimed to continue the spectropolarimetric monitoring of Of?p stars located in the LMC and SMC (see Paper I), and one aimed at searching for magnetic fields in the most massive stars.

With very few exceptions, observations were obtained in polarised multi-object spectroscopy (PMOS) modes, using grism 1200B. FORS2 MOS employs a system of mechanical slitlets that can be translated along horizontal tracks. In PMOS mode, nine independent slitlets are available over a $6.8' \times 6.8'$ field of view. In addition, the instrument can be rotated, providing two degrees of freedom to position the slitlets. Typically, the observing procedure for PMOS is to fill as many slitlets as possible with primary targets, which are constrained by the position of the targets in the field, and then to fill the remainder with secondary targets with brightnesses comparable to those of the primary targets. As a consequence, we obtained a mix of observations of primary targets and other stars in the field. The actual spectral range depends on the position of the MOS slitlet in the field of view; with the slit in a central position, it was 3700–5120 Å.

The observing programme on extra-galactic Of?p stars was carried out in visitor mode from 20 to 24 November 2017 (programme ID 100.D-0670). The primary targets of this programme were the Of?p stars SMC 159-2 and AzV 220, which were already observed in Paper I, and the newly discovered extra-galactic Of?p star LMCe 136-1 (Neugent et al. 2018). Most of these observations were carried out in multi-object spectropolarimetric mode with grism 1200B; however, during one night, the star SMC 159-2 was observed in single object (“fast”) mode. In addition, spectroscopic-mode (long-slit) observations of these Of?p stars were obtained with grism 1200R to monitor the variability of their H α line. Since our hot and weakly reddened targets emit more flux in the blue than in the red and since the blue spectral region is much richer in lines than the red spectral region, for these observations, we employed the EEV CCD (previously used in the now decommissioned FORS1 instrument), which is optimised in the blue. All the observed targets are summarised in Table A.1.

Observations of reference magnetic stars are not included in the standard FORS2 calibration plan; nevertheless, they are needed to confirm that the position angle of the retarder waveplate is correctly reported by the instrument encoders. For this

Table 1. New EW measurements obtained with grisms 1200B and 1200R.

STAR	DATE	UT	Line	EW (Å)
SMC 159-2	2017-11-21	02:53	He II 4686	-3.65 ± 0.09
			H β	-1.82 ± 0.09
	2017-11-21	00:32	H α	-11.02
			He II 4686	-4.21 ± 0.08
	2017-11-22	01:28	H β	-2.29 ± 0.07
			H α	-15.50
2017-11-24	02:25	He II 4686	-4.76 ± 0.05	
		H β	-2.84 ± 0.06	
2017-11-24	00:53	H α	-19.72 ± 0.17	
LMCe 136-1	2017-11-21	06:40	He II 4686	-2.36 ± 0.03
			H β	-1.09 ± 0.03
	2017-11-21	08:24	H α	-7.72 ± 0.12
			He II 4686	-2.46
	2017-11-22	08:20	H β	-1.36
			H α	-7.66
2017-11-23	07:39	He II 4686	-2.44 ± 0.04	
		H β	-1.54 ± 0.03	
2017-11-23	08:43	H α	-8.70	
LMC 164-2	2017-11-22	07:51	He II 4686	-1.47
			H β	-0.47
2017-11-22	08:31	H α	-3.25	
AzV 220	2017-11-24	04:51	He II 4686	-1.33 ± 0.02
			H β	-1.94 ± 0.04

Notes. Uncertainties were estimated from the standard deviation of the measurements of multiple frames (hence they are not reported when obtained from a single frame only).

reason, we decided to use some of the twilight time to observe two well-known and bright magnetic Ap stars: HD 94660, which has an almost constant longitudinal magnetic field of -2 kG (e.g. Landstreet et al. 2014), and HD 188041, which has a well-known magnetic curve that varies with a period of 223.78 d (Landstreet & Mathys 2000) and has been observed for more than 60 yr, beginning with Babcock (1954).

A second observing programme (programme ID 094.D-0533) was aimed to study the magnetic properties of the most massive known stars. This programme focused on the 30 Dor region in the LMC, a region that has also been extensively studied as part of the VLT-FLAMES Tarantula Survey (VFTS; Evans et al. 2011). The EEV CCD is not offered in service mode; therefore, we used the MIT CCD, which is optimised for the red. Our main targets were Mk 25 and Mk 51 in NGC 2070 (Melnick 1985), R136b and c in R136 (Feitzinger et al. 1980; Schnurr et al. 2009) and others situated further out (e.g. VFTS 682; Bestenlehner et al. 2011), and NGC 3603, which hosts several well-known massive stars (e.g. NGC 3603a1, B and C; Moffat et al. 2004; Melena et al. 2008; Crowther et al. 2010). Ultimately only a sub-sample of the original targets were observed: VFTS 621 (in “Knot 2” from Walborn & Blades 1987) = Walborn 2 ($M = 104 M_{\odot}$), VFTS 506 = Mk 25 ($M = 138 M_{\odot}$, both mass values from Sabín-Sanjulián et al. 2014), R136c = VFTS 1025 ($M = 132 M_{\odot}$), Mk37Wa = VFTS 1021 ($M = 141 M_{\odot}$), VFTS 457 = Mk 51 ($M = 100 M_{\odot}$), VFTS 682 ($M = 153 M_{\odot}$), and Mk 42 = BAT 99 105 = Brey 77 ($M = 153 M_{\odot}$, all five values from Bestenlehner et al. 2014). In addition to these

primary targets, as explained before, nearby stars were used to fill the unoccupied MOS slitlets. These secondary targets were mostly O-type and WR stars, along with a few later-type supergiants. The targets observed in the context of this programme are summarised in Table A.2.

The photometric data used in this analysis were obtained by the Optical Gravitational Lensing Experiment (OGLE) project, which was realised on the 1.3 m Warsaw Telescope located in Las Campanas Observatory, Chile, and operated by the Carnegie Institution for Science during its second, third, and fourth phases (1997–2019, Udalski et al. 2015).

3. Data reduction, magnetic field diagnosis, and quality checks

Data were reduced using the method explained by Bagnulo et al. (2015). The mean longitudinal magnetic field $\langle B_z \rangle$ (i.e. the component of the magnetic field averaged over the visible stellar disc) was calculated by minimising the expression

$$\chi^2 = \sum_i \frac{(y_i - \langle B_z \rangle x_i - b)^2}{\sigma_i^2} \quad (1)$$

where, for each spectral point i , y_i is the reduced Stokes parameter $V/I = P_V(\lambda_i)$ and $x_i = -g_{\text{eff}} c_z \lambda_i^2 (1/I) dI/d\lambda_i$; g_{eff} is the effective Landé factor, c_z is a constant $\approx 4.67 \cdot 10^{-13} \text{ \AA}^{-1} \text{ G}^{-1}$ (see Bagnulo et al. 2002), λ is the wavelength measured in \AA , and b is a free parameter introduced to account for possible spurious polarisation in the continuum. As a quality check, field measurements were also estimated from the null profiles (see Bagnulo et al. 2012, for an extensive discussion on the use of null profiles for quality control).

For the field measurement, we considered three cases: in Eq. (1) we first used the spectral points and only included H Balmer lines (adopting $g_{\text{eff}} = 1$ for the Landé factor; Casini & Landi Degl’Innocenti 1994), then we only included He and metal lines (setting for metal lines on the average value of $g_{\text{eff}} = 1.25$), and finally we included all spectral lines together (H, He, and metal). However, if lines showed obvious emission, we avoided them so as to probe the stellar photosphere rather than the circumstellar environment, unless only emission lines were present in the stellar spectrum, which is similar to the case of WR stars. As the results of these three measurement procedures roughly agree, here, we only report the last value, which also yields the smallest error bars. We also measured the so-called null field $\langle N_z \rangle$ by minimising the expression of the χ^2 of Eq. (1) using the null profiles N_V (Donati et al. 1997; Bagnulo et al. 2009) instead of the reduced Stokes profiles P_V . The null profiles are essentially defined as the difference between reduced Stokes parameters obtained from different pairs of measurements, and they represent an experimental estimate of the noise. We expect null profiles and null field values to be consistent with zero within their photon-noise uncertainty. A deviation from zero reveals the presence of significant non-photon noise, while consistency with zero does not guarantee that systematic errors are still absent from the data. For a definition and full discussion of the use of the null profiles and null fields as a quality check, see Bagnulo et al. (2012, 2013).

4. Results

In total, we observed 41 science targets (some of them multiple times), including Of?p stars, cool supergiants, main sequence

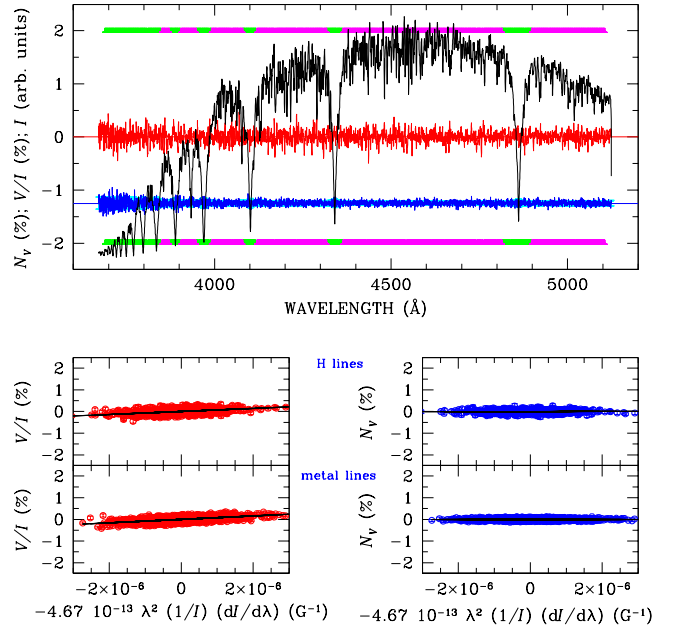


Fig. 1. FORS2 observations of the magnetic reference Ap star HD 188041. In the *upper panel*, the black solid line shows the Stokes I spectrum (uncorrected for the transmission function of the atmosphere + telescope and instrument optics); the red solid line shows the reduced Stokes V spectrum, $P_V = V/I$ (in % units), and the blue solid line is the null profile offset by -1.25% for display purposes. The scattering of the null profile about zero is consistent with the 1σ photon-noise uncertainties, which are also shown centred around -1.25% and appear as a light blue background to the null profile. Spectral regions highlighted by green bars (at the top and bottom of the panel) have been used to determine the $\langle B_z \rangle$ value from H Balmer lines, while the magenta bars highlight the spectral regions used to estimate the magnetic field from He and metal lines. *Four bottom panels*: best-fit obtained by minimising the χ^2 expression of Eq. (1) using the P_V spectra (*left panels*) and the N_V spectra (*right panels*) for H Balmer lines (*upper panels*) and metal lines (*lower panels*).

OB stars, evolved OB stars, and WR stars. The results for each of these groups are discussed in Sects. 5.1–5.4. In addition, two well-known magnetic Ap stars were also observed to check the correct alignment of the polarimetric optics, namely HD 94660 and HD 188041. Figure 1 shows an example of field detection on one of the magnetic reference stars (HD 188041), and Fig. 2 shows the same plots for the Of?p targets LMCe 136-1, SMC 159-2, and AzV 220. Our full list of magnetic measurements is given in Tables A.1 and A.2.

In addition to the magnetic field measurements, for the Of?p stars of our target list, we also measured the equivalent widths (EWs) of He II 4686, H β , and H α (see Table 1 and Fig. 5); these measurements are discussed in Sect. 5.1.

4.1. Observations of magnetic reference stars

Our field measurement of HD 94660 ($\langle B_z \rangle = -2345 \pm 45 \text{ G}$) is consistent with the expected value from previous measurements published in the literature (the star exhibits a longitudinal field that oscillates around -2 kG , see Bagnulo et al. 2012, and references therein), and so were the field measurements of HD 188041 ($\langle B_z \rangle = 770 \pm 20 \text{ G}$ on the nights of 20 to 21 November 2017 and $780 \pm 20 \text{ G}$ on the nights of 21 to 22 November 2017). Phased with the ephemeris of Landstreet & Mathys (2000), our measurements of HD 188041 appear to have been taken close to the

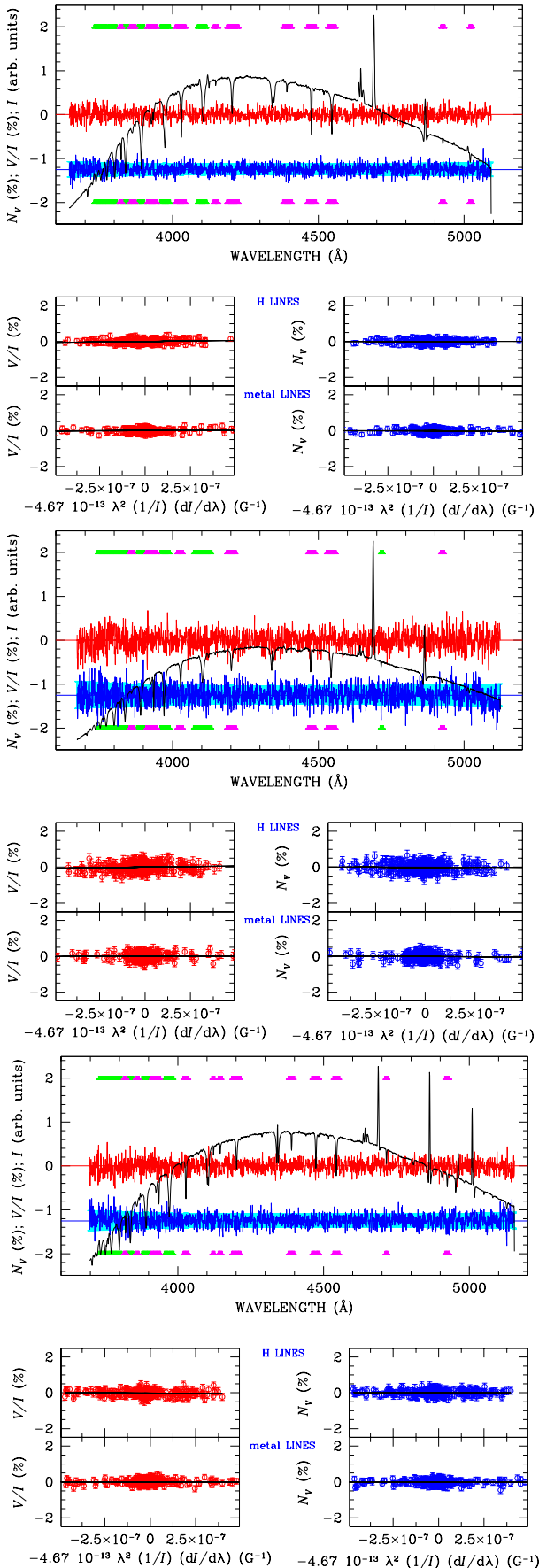


Fig. 2. Same as Fig. 1 for three of our science targets: LMCe 136-1 (*top panels*), SMC 159-2 (*mid-panels*) and AzV 220 (*bottom panels*).

magnetic minimum and, similar to what was found in Paper I, they are ~ 200 G higher compared to the measurements obtained by Babcock (1954, 1958) at similar rotation phases. These discrepancies do not suggest a problem with the instrument, but, as discussed in detail by Landstreet et al. (2014), they are rather a symptom of the systematic differences that are present when the longitudinal field is measured with different instruments and even simply different setups.

4.2. Magnetic field measurements of the science targets

Our field measurements summarised in Tables A.1 and A.2 mainly represent non-detections, but there are some occasional $\sim 3\sigma$ detections, both from the reduced Stokes V profiles and from the null profiles. As discussed by Bagnulo et al. (2012), spectropolarimetry with Cassegrain-focus mounted instruments is less accurate than what can be obtained with a fibre-fed instrument that is specifically designed for accurate radial velocity measurements (e.g. ESPaDOnS at the CHFT and HARPS at the 3.6 m telescope of the La Silla Observatory). The reason is that even tiny instrument flexures occurring over the course of an exposure series may be responsible for spurious signals that mimic a Zeeman signature, especially on relatively narrow spectral lines (see Fig. 1 of Bagnulo et al. 2013). The situation is even more likely to occur during particularly long exposures at high airmass, such as those obtained during the run dedicated to the Of?p stars. Spurious results may also occur more frequently in the presence of blending, such as in the case of many of those observed in the run dedicated to the very massive stars. The reason is that seeing variations may change the appearance of spectral features during the observing series. Therefore, the occurrence of marginal detections on null profiles is not particularly surprising. For the same reason, our marginal $\langle B_z \rangle$ detections on the reduced V profiles do not necessarily suggest the presence of a magnetic field. An overall view of the distribution of our $\langle N_z \rangle$ and $\langle B_z \rangle$ measurements, which are normalised by their uncertainties, is given in Fig. 3. In the ideal case, the distribution of the quantities $\langle N_z \rangle / \sigma_{\langle N_z \rangle}$ should be similar to a Gaussian distribution with $\sigma = 1$. In fact, the $\langle N_z \rangle / \sigma_{\langle N_z \rangle}$ histograms display a larger width, with some $\langle N_z \rangle$ detections at 3σ level. This suggests that also the various marginal ($\sim 3\sigma$) $\langle B_z \rangle$ detections should be treated with caution and they should not be considered to be conclusive. In conclusion, the uncertainties declared in our result tables do not fully account for non-photon noise, which although apparent in the global analysis of all measurements, is difficult to quantify for individual stars.

4.3. Uncertainties of the field measurements versus S/N

Figure 4 combines previous results obtained with bright (Galactic) O-type stars observed with FORS1 (shown in Fig. 5 of Bagnulo et al. 2015) with the data of extra-galactic Of?p stars presented here and in Paper I. The top panel shows the uncertainties of our field measurements versus S/N; the bottom panel shows the predictions of the FORS2 exposure time calculator (ETC) for the S/N on $V = 14$ – 15.5 magnitude stars that can be reached as a function of the exposure time as well as the S/N that was actually reached in our observations. Discrepancies between ETC predictions and real observations are due, in part, to less-than-ideal weather conditions and also to the fact that the ETC is optimistic regarding the instrument performances in polarimetric mode. Nevertheless, detection at a 5σ confidence level of a magnetic field in an O-type star of the MC with a dipolar field

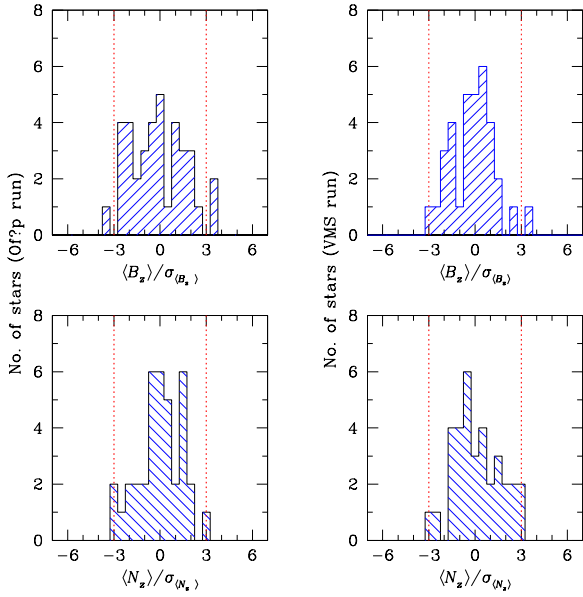


Fig. 3. Distribution of $\langle B_z \rangle$ and $\langle N_z \rangle$ values normalised to their uncertainties for the stars observed during the run dedicated to Of?p stars (*left panels*) and for the stars observed during the run dedicated to the VMS stars (*right panels*). The vertical dotted lines mark the $3\text{-}\sigma$ limits of these distributions.

$\geq 1500\text{--}2000$ G should be just within the limits of the capabilities of the FORS2 instrument if the star is observed in favourable conditions. Indeed, it should be taken into account that a star could have a very strong surface magnetic field, but, for geometrical reasons, have a zero average longitudinal component at the time of the observation. More generally, a single null measurement of the longitudinal field only provides limited constraints on the star's surface dipole field strength. However, when combined together, several measurements on the same target may provide a useful estimate of the upper limit of the star's dipolar field strength. In the next section, we use a statistical approach that proves to be especially useful when no direct modelling of the data are possible (e.g. due to scarcity of data or to the fact that all field measurements are non-detections).

5. Constraints on the magnetic field strength of the observed extra-galactic stars

The problem of how to estimate an upper limit for the field strength from a series of non-detections has been tackled using approaches of both Bayesian (e.g. [Kolenberg & Bagnulo 2009](#); [Petit & Wade 2012](#); and [Asensio Ramos et al. 2014](#)) and classical (frequentist) statistics (e.g. [Neiner et al. 2015b](#)). Here, we follow a Bayesian approach, extending the use of Eq. (7) of [Kolenberg & Bagnulo \(2009\)](#) to an arbitrary number of field measurements (see also Sect. 3.2 of [Petit & Wade 2012](#)). We calculate the probability \mathcal{P} that, given a set of $\langle B_z \rangle_j \pm \sigma_j$ measurements, the strength of the dipolar field B_{dip} is within the range $[B_1, B_2]$. Equation (7) of [Kolenberg & Bagnulo \(2009\)](#) becomes

$$\begin{aligned} \mathcal{P}(B_1 \leq B_{\text{dip}} \leq B_2) &\propto \int_{B_{\text{dip}}} \int_i \int_\beta p_B(B_{\text{dip}}) \sin i \sin \beta \prod_j \int_{f_j} \\ &\exp\left(-\frac{(\langle B_z \rangle_j - k(u)B_{\text{dip}}[\cos i \cos \beta + \sin i \sin \beta \cos f_j])^2}{2\sigma_j^2}\right) \end{aligned} \quad (2)$$

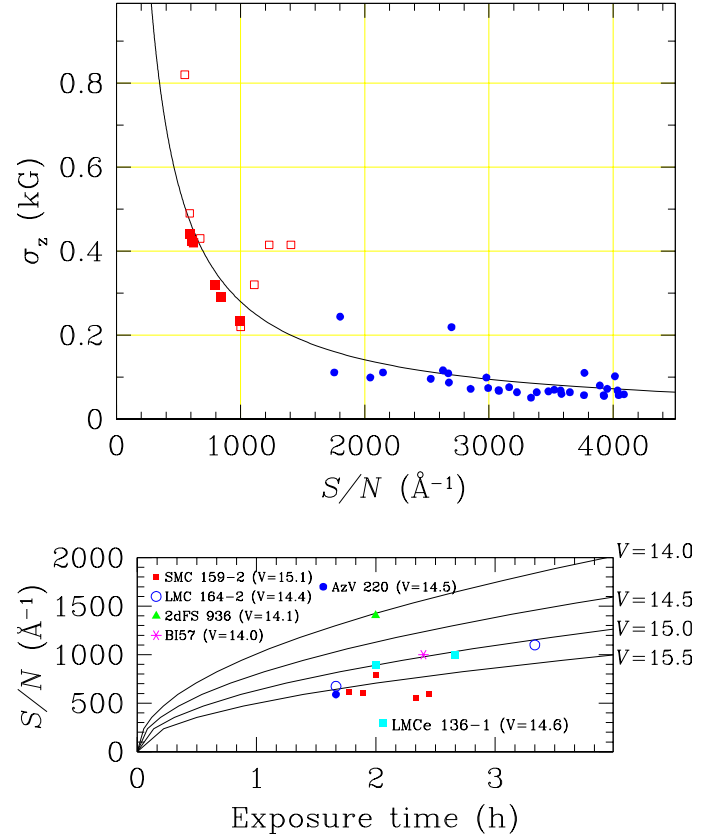


Fig. 4. *Top panel:* uncertainties of the field measurements obtained with the FORS1/2 instruments for various O-type stars. Blue filled circles refer to bright Galactic O-type stars observed with FORS1 (see [Bagnulo et al. 2015](#)); red empty squares correspond to LMC/SMC O-type stars observed with FORS2 in Paper I and red filled squares LMC/SMC O-type stars observed with FORS2 and presented in this paper. The solid line is the best hyperbolic fit to the data points. *Bottom panel:* S/N vs. exposure time. Symbols refer to different observations of O-type stars as explained in the legend. Solid lines show the predictions of ETC version P103.2 for a O5 star observed at airmass = 1.5 with grism 1200B through a $1''$ slit width, with $1.0''$ seeing, and fraction of lunar illumination = 0.5.

where i , the tilt angle between line of sight and rotation axis, and β , the angle between rotation axis and magnetic field axis, are assumed to be isotropic; the prior probability densities of phase f_j are constant; for the B_{dip} distribution, we assume p_B is a modified Jeffreys prior (e.g. [Petit & Wade 2012](#)); and $k(u)$ is a constant that depends on the limb-darkening coefficient u (assuming $u = 0.5$ we have $k = 0.31$). Practically speaking, for most of the cases of this paper, we are primarily interested in the upper limit $B_{\text{dip}}^{(\text{max})}$ of the dipolar field strength defined such that there is a 95% probability that the dipolar field B_{dip} at the magnetic pole of the star is smaller than $B_{\text{dip}}^{(\text{max})}$ if the star is magnetic. This estimate of $B_{\text{dip}}^{(\text{max})}$ alone does not, however, tell us whether the star is likely to be magnetic or not. Instead, the likelihood that a magnetic field is present may be estimated by the odds ratio (see Eq. (3.14) of [Gregory 2005](#)). Following [Petit & Wade \(2012\)](#), we affirm that there is no evidence for a magnetic field if the odds ratio is ≤ 3 and that there is weak, moderate, strong, or very strong evidence that the star is magnetic if the odds ratio is between 3 and 10, 10 and 30, 30 and 100, and ≥ 100 , respectively. As a quality check, we also applied these concepts of Bayesian statistics to the null field values and derived the corresponding

maximum dipolar field strength $N_{\text{dip}}^{(\text{max})}$. Similar to what is discussed for the individual $\langle N_z \rangle$ values by Bagnulo et al. (2012), the values obtained from the $\langle N_z \rangle$ values should not be interpreted as errors on the $B_{\text{dip}}^{(\text{max})}$ values; although from the $\langle N_z \rangle$ values, we should expect to find no evidence for the presence of a magnetic field.

For three Of?p stars for which we have more than one magnetic field measurement, we have a good estimate of the rotational period; therefore, the relative phase of each measurement is also known, that is, $f_j = f + \phi_j$ for known ϕ_j . If we assume that the magnetic field maximum occurs at the same time as the maximum of the light curve (e.g. Munoz et al. 2020), we can also deduce the rotational phase at which our field measurements were obtained. If the star’s rotation period is known, but not the epoch of the maximum of $\langle B_z \rangle$, the product of $N f_j$ -integrals in Eq. (2) is replaced by a single integral over f , and if the absolute value of the phase is also known, there is no phase integral. Further analysis of this approach will be provided by Asher & Bagnulo (in prep.).

In the following, we apply this method to the stars of our target list, which include Of?p stars (Sect. 5.1), early-type, and late-type main sequence and supergiants (Sect. 5.3), main sequence OB stars (Sect 5.2), and WR stars (Sect 5.4). Our targets range in apparent V magnitude from 11.3 (the red supergiant candidate TYC 8891-3239-1; Neugent et al. 2012) to 16.2 (luminosity class III-V B-type stars). For the majority of objects, the individual measurements of magnetic fields have uncertainties of a few hundred Gauss; the limitation of the precision is not really due to stellar luminosities but the lack of absorption lines. The estimated upper limits of the dipolar field strengths for all stars observed at least twice (also including the data collected in Paper I) are given in Table 2. Generally, these upper limits were estimated assuming that each measurement was obtained at a random value of the rotational phase, which is the only possibility when the star’s rotation period is unknown. For three Of?p stars, we could also estimate these upper limits using the constraint given by their rotation period. In this situation we know the phase offset between each field measurement (case “relative” in Table 2). Under the hypothesis that the maximum of the light curve coincides with the maximum of the longitudinal magnetic field, we can also make the further assumption of knowing at which position of the magnetic curve each field measurement was obtained (case “absolute” in Table 2).

5.1. Of?p stars

The Of?p stars of our target list are probably the best magnetic candidates and deserve to be discussed individually.

5.1.1. SMC 159-2

SMC 159-2 was identified as an Of?p star by Massey et al. (2014). Nazé et al. (2015) investigated the photometry of this star and establish clear 14.914 ± 0.004 d periodic variability. In Paper I, we demonstrate that the EWs of $H\beta$ and He II $\lambda 4686$ varied smoothly according to this same period. Using the most recent epochs of OGLE photometry, we derived a new ephemeris for SMC 159-2, with $T_0 = 2457416.997$ and $P = 14.915 \pm 0.003$ d. This ephemeris is sufficiently precise to allow us to phase our new EWs, measured from He II $\lambda 4686$, $H\beta$ and $H\alpha$, with those of Bagnulo et al. (2017). The resultant phase curves, illustrated in Fig. 5, show an emission maximum occurring at

Table 2. Limits for the dipolar field strength obtained through Bayesian statistical considerations.

STAR	$B_{\text{dip}}^{(\text{max})}$		$N_{\text{dip}}^{(\text{max})}$	
Of?p:				
AzV 220	2325	N	8825	N
SMC 159-2	12 125	m	10725	N
SMC 159-2 (relative)	10 075	s	7275	N
SMC 159-2 (absolute)	11 275	vs	9825	N
LMCe 136-1	2825	N	1375	N
LMCe 136-1 (relative)	3225	N	1475	N
LMCe 136-1 (absolute)	4625	N	2275	N
LMC 164-2	3775	N	7975	N
LMC 164-2 (relative)	3775	N	7975	N
LMC 164-2 (absolute)	6725	N	2525	N
OB supergiants:				
Mk 42 (VMS)	3725	N	1825	N
VFTS 526	7975	N	5725	N
Mk37Wa (VMS)	6925	N	8825	N
VFTS 291	4275	N	6175	N
VFTS 458	2075	N	3525	N
BA giants:				
NGC 346 ELS 1080	9475	N	5375	N
NGC 346 ELS 19	7025	N	6075	N
OB dwarfs:				
VFTS 441	5875	N	4875	N
VFTS 500	7075	N	18925	w
VFTS 506 (VMS)	2474	N	3575	N
VFTS 586	12 285	N	5565	N
VFTS 621 (VMS)	1525	N	1275	N
VFTS 589	9025	N	7225	N
AzV 55	1025	N	975	N
AzV 66	1325	N	2075	N
2dFS 5037	8925	N	4375	N
2dFS 5038	1675	N	1225	N
NGC 346 ELS 27	12 975	N	4475	N
NGC 346 ELS 68	6525	N	5525	N
NGC 346 ELS 100	5075	N	8625	N
NGC 346 ELS 103	3275	N	16675	N
Cool supergiants:				
W60 D24	175	N	225	N
RM 1-546	775	N	775	N
SkKM 179	3025	N	575	N
VFTS 341	1075	N	625	N
CPD-69 463	1175	N	775	N
WR:				
VFTS 507	925	N	1425	N
VFTS 509	1175	N	1825	N
R 136c (VMS)	12 675	N	5575	N
VFTS 682 (VMS)	2975	N	3075	N

Notes. Column 2 reports the $B_{\text{dip}}^{(\text{max})}$ value, and the flag of Col. 3 means no (N), weak (w), moderate (m), strong (s), or very strong (vs) evidence for the presence of a magnetic field. Columns 4 and 5 as Cols. 2 and 3, but for the null field values. The meaning of relative and absolute refers to results obtained assuming that the star’s rotation period is known, as explained in the text.

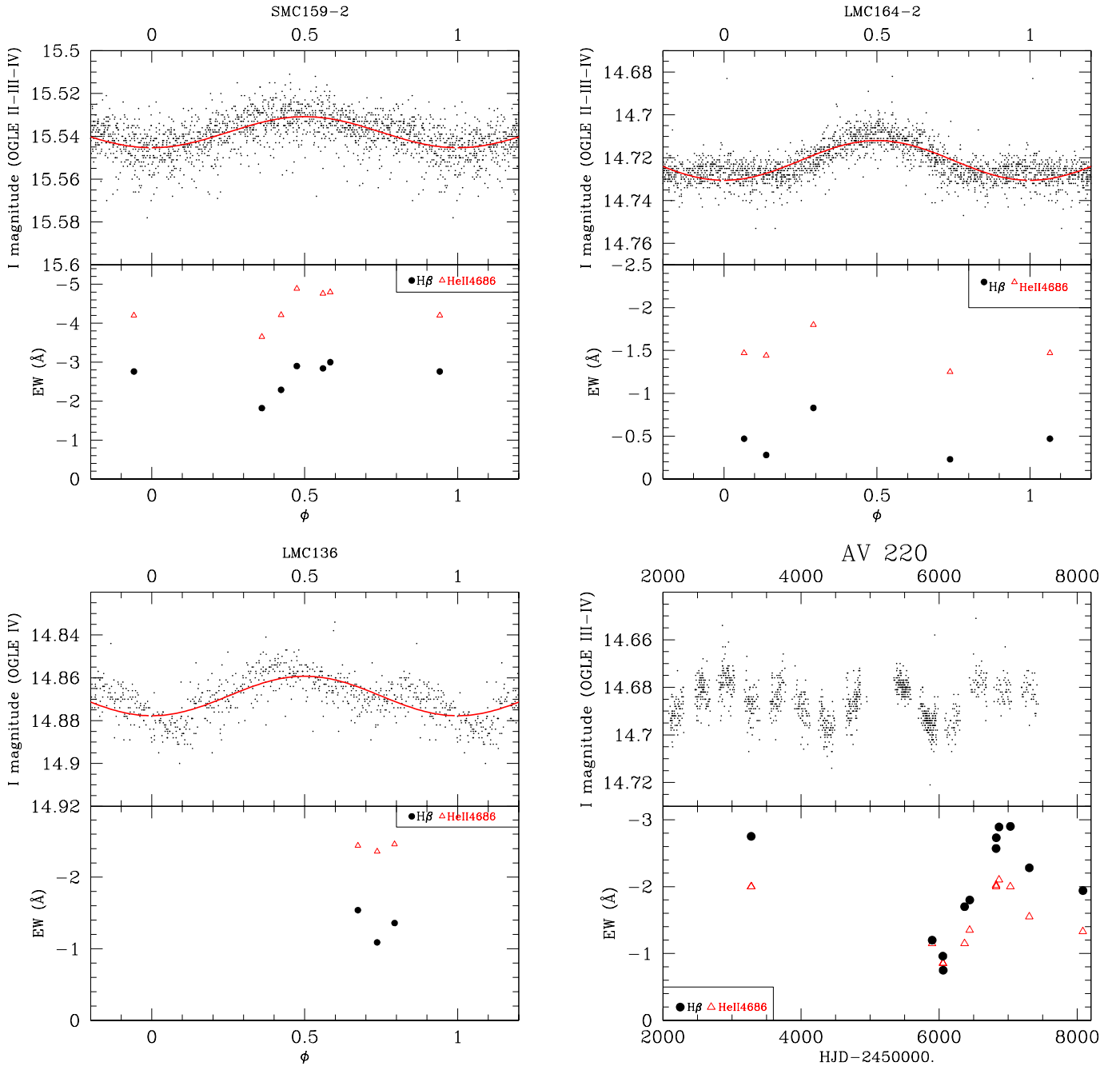


Fig. 5. Comparison of photometric measurements with equivalent widths of four extra-galactic Of?p stars. *Top left panel:* SMC 159-2; *top right panel:* LMC 164-2; *bottom left panel:* LMCe 136-1; *bottom right panel:* AzV 220. Symbols refer to H β (black solid circles) and He II λ 4686 (empty red triangles). Equivalent width data are from Table 1, from Bagnulo et al. (2017), and the references therein. Photometric data are from OGLE.

approximately the same phase as maximum brightness. Such a relative phasing is qualitatively consistent with the rotational modulation of a stellar magnetosphere (see e.g. Munoz et al. 2020 and Driessen et al. 2018).

In Paper I, we measured a longitudinal field of 2.8 ± 1 kG, which is nearly a 3σ detection of a 3 kG longitudinal field. In view of the considerations of Sect. 4.2, this measurement is probably too marginal to be considered to be a reliable detection. In this work, we obtain four new polarimetric measurements (two of which sequentially on a single night), all are close to maximum emission as is the measurement presented in Paper I. Compared to the observations presented in Paper I, which were obtained

with similar exposure times, our new measurement uncertainties are lower because of much better weather conditions. None of the measurements yield a significant detection of the longitudinal field, with a best uncertainty of 270 G, but they are all of a positive sign, and roughly consistent with each other (as expected when obtained at a similar rotation phase if the star is magnetic). Figure 6 shows our $\langle B_z \rangle$ and $\langle N_z \rangle$ measurements of this star as a function of the star's rotational phase.

Although none of our measurements may be considered to be a detection, the results of a Bayesian statistical analysis lead to the suggestion that the star possesses a magnetic field. First we consider the case in which we do not use the star's rotation period

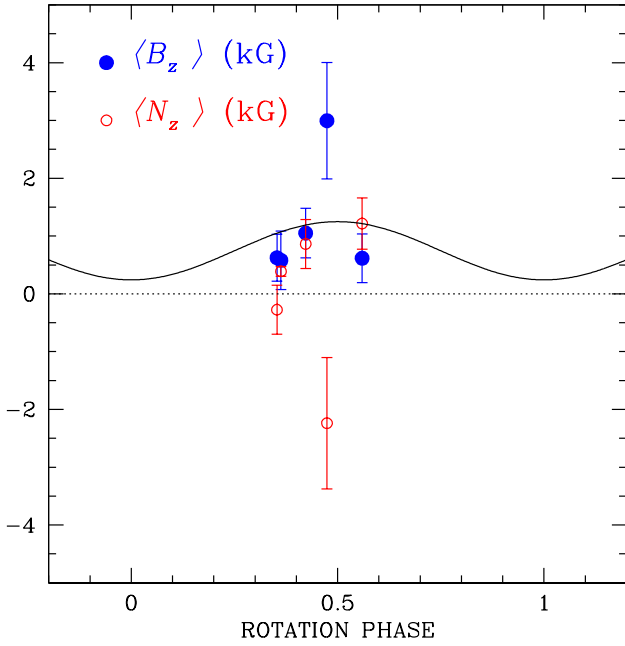


Fig. 6. Mean longitudinal field and null field measurements of SMC 159-2 as a function of the rotational phase. Here the rotation phase is defined consistently with the light curves of Fig. 5, which is offset by 0.5 cycles from what is usually adopted for longitudinal field curves (which generally have the maximum at rotation phase zero). The field measurement at rotation phase =0.5 was presented in Paper I. The solid curve shows the prediction of the model by Munoz et al. (2020).

as a constraint, that is, we assume that all field measurements were obtained at an unknown rotational phase. In this situation, the two consecutive measurements obtained on the night of 21 November 2017 were averaged out and we considered a total of four field measurements. The odds ratio, that is, the probability that the star is magnetic versus the probability that there is no magnetic field is ~ 13 , which corresponds to “moderate” evidence for the presence of a magnetic field; the probability distribution function (PDF) of the dipolar field strength is smooth, and it tells us that there is a 50% probability that the dipolar field strength at the pole is between 0 and 5 kG, or a 95% probability that the dipolar field strength at the pole is between 0 and 12 kG. If we use the star’s rotation period as a constraint, and we assume that the mean longitudinal field has a maximum when the EW has a maximum, then the odds ratio is ~ 140 , corresponding to very strong evidence for the presence of a magnetic field. This reflects the fact that our five measurements all have the same sign and are all close in the rotation phase (within three days over a 15 day rotation period). On the other hand, there are two negative and three positive ($\langle N_z \rangle$) values in Table A.1. This set of values is consistent with the zero field (thus “no evidence” in Table 2), while also being consistent with a significant $N_{\text{dip}}^{(\text{max})}$ value. The B_{dip} PDF tells us that there is a 50% probability that the dipolar field strength at the pole is comprised between 2.4 and 4.4 kG, and a 95% probability that is between 0 and 11 kG. These predictions are consistent with those by Munoz et al. (2020), who used the analytic dynamical magnetosphere (ADM) model of Owocki et al. (2016) to compute synthetic lightcurves of four Of?p stars in the Magellanic Clouds, including SMC 159-2. Comparing their model to the data of SMC 159-2, Munoz et al. (2020) predict a surface dipole field strength of $6.4_{-1.8}^{+3.5}$ kG.

5.1.2. LMC 164-2

LMC 164-2 was also identified as an Of?p star by Massey et al. (2014). Nazé et al. (2015) established clear 7.9606 ± 0.0010 d periodic variability. In Paper I, the EWs of H β and He II $\lambda 4686$ are shown to be compatible with this period.

In Paper I, we measured $\langle B_z \rangle = 0.20 \pm 0.56$ kG and -0.55 ± 0.90 kG in this star (i.e. we did not detect a magnetic field). In the present paper, we did not obtain any new field measurements of LMC 164-2, but we did measure new EWs of the H β and H α profiles.

Using the most recent epochs of OGLE photometry, we derived a new ephemeris for LMC 164-2, with $T_0 = 2457506.140$ and $P = 7.9606 \pm 0.0009$ d. This ephemeris is sufficiently precise to allow us to phase our new EWs with those of Bagnulo et al. (2017). The resultant phase curves, illustrated in Fig. 5, appear coherent, but the measurements are too sparse to allow us to evaluate any relationship between the EWs and the stellar brightness in detail.

From the field measurements obtained in Paper I, and assuming that the observations were obtained at unknown rotation phases, we estimate that the upper limit of the dipole field is 3.8 kG. Assuming that the rotation phase is known with respect to the magnetic maximum, the constraint on the dipole field is weaker: There is a 95% probability that the dipolar field strength is between 0 and 6.7 kG. In any case, our data do not provide evidence that the star is magnetic. We note that the assumption that we know the absolute rotational phase leads to higher $B_{\text{dip}}^{(\text{max})}$ values than in the relative case. One could expect that the former assumption should offer tighter constraints on the $B_{\text{dip}}^{(\text{max})}$ values, rather than looser constraints. In this case, this expectation is not met. For LMC 164-2, we obtain two measurements that are approximately separated by 0.5 rotational cycles. If we set no constraints on the absolute value of the rotation phase, then we must allow for the possibility that the measurement of $\langle B_z \rangle \sim -0.5$ kG was obtained close to magnetic maximum and the measurement of approximately +0.2 kG was obtained close to the magnetic minimum, a situation that necessarily requires a low B_{dip} value. If we introduce the constraint that $\langle B_z \rangle \sim +0.2$ kG was obtained close to magnetic maximum and $\langle B_z \rangle \sim -0.5$ kG was obtained close to the magnetic minimum, as we effectively did in the absolute case, then the close-to-zero B_{dip} values have a lower statistical weight than in the relative case. We should note, however, that the parameter $B_{\text{dip}}^{(\text{max})}$ alone does not suffice to characterise the PDF, and that a comparison between different $B_{\text{dip}}^{(\text{max})}$ values does not fully describe the difference between PDFs.

The ADM modelling performed by Munoz et al. (2020) indicates that the star’s surface magnetic dipole should be $B_{\text{dip}} = 12.3_{-0.5}^{+1.8}$ kG, which is higher by a factor of 2 as compared to the upper limit derived here. The reason for this discrepancy is that in order to estimate the dipolar field strength, Munoz et al. (2020) also used photometric data, a constraint that is not taken into account here. Clearly, more spectropolarimetric data are needed to set more meaningful constraints on the magnetic geometry of LMC 164-2.

5.1.3. LMCe 136-1

This new Of?p star ($\alpha = 05:32:22.85$, $\delta = -67:10:18.5$ in J2000) was found by Neugent et al. (2018). It was observed in the OGLE IV survey (Udalski et al. 2015), and photometry was derived with the differential image analysis (DIA) method.

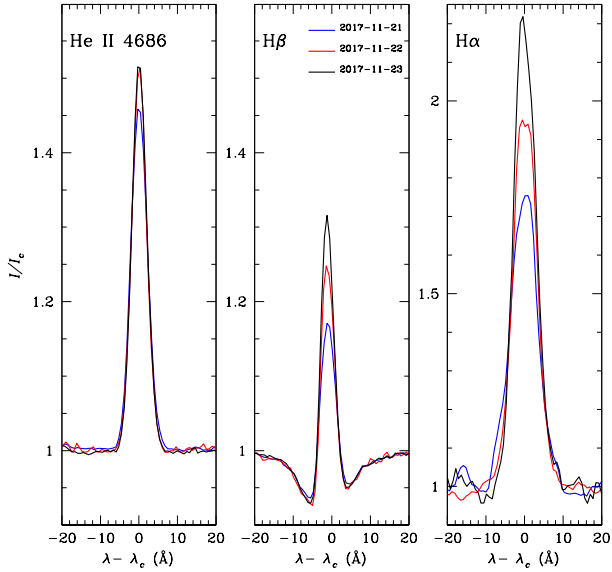


Fig. 7. Stokes I profiles (normalised to the continuum) for the spectral lines He II $\lambda 4686$ (left panel), $H\beta$ (mid panel), and $H\alpha$ (right panel) of LMCe 136-1 observed in three consecutive nights.

We analysed this dataset using the procedures of Nazé et al. (2015) and found a clear period of 18.706 ± 0.016 d, with $T_0 = 2457\,503.827$. LMCe 136-1 is thus an analogue of SMC 159-1 and LMC 164-2. The spectropolarimetric data were all obtained at roughly the same phases between maximum and minimum brightness. The EWs measured from these spectra are variable (see Fig. 7), as expected.

The photometry and EWs as a function of rotation phase are illustrated in Fig. 5. As with LMC 164-2, the EW measurements are too sparse to establish any relationship between the photometric and spectroscopic variations.

The longitudinal field measurements all correspond to null detections ($\langle B_z \rangle = 450 \pm 235$ G and -85 ± 275 G). Taken all together, they do not prove the existence of a magnetic field and set an upper limit on the dipolar field of $B_{\text{dip}}^{(\text{max})} = 4.5$ kG. This is consistent with the surface magnetic dipole strength inferred by Munoz et al. (2020), $B_{\text{dip}} = 5.6_{-1.9}^{+4.1}$ kG.

5.1.4. AzV 220

AzV 220 was identified as an Of?p star by Walborn et al. (2000) and confirmed by Massey & Duffy (2001). Nazé et al. (2015) establish photometric variability, but they were unable to derive a period. Walborn et al. (2015) report 11 spectra of AzV 220, confirming clear long-term variability of $H\beta$ and He II $\lambda 4686$. In Paper I, we report two new EWs of $H\beta$ and He II $\lambda 4686$. Our new $H\beta$ and $H\alpha$ EWs demonstrate that AzV 220 continues to exhibit significant and likely complex long-term variability. No period is yet discernible.

Our single measurement of the longitudinal field of AzV 220 in Paper I yields a null result with a ~ 0.6 kG uncertainty. In the present paper, we obtain one new polarimetric measurement of AzV 220: a null result of 0.2 ± 0.3 kG. Altogether, they set an upper limit to the dipolar field strength of $B_{\text{dip}}^{(\text{max})} = 2.3$ kG.

5.2. Main sequence and evolved OBA stars

Both observing campaigns used main sequence and evolved OBA stars to fill unoccupied slitlets. In the VMS fields, these

include (i) the O supergiants VFTS 457, Brey 77 (= Mk 42), VFTS 526, and Mk 37Wa; (ii) the B supergiants VFTS 291 and VFTS 458; (iii) the O dwarfs VFTS 441, VFTS 500, VFTS 506, VFTS 586, and VFTS 621; and (iv) the B dwarf VFTS 589. In the Of?p fields, these include (v) the B dwarfs AzV 55 and AzV 66; (vi) the A giant NGC 346 ELS 19, (vii) the OB dwarfs NGC 346 ELS 27, NGC 346 ESL 68, NGC 346 ELS 100, NGC 346 ELS 103, 2dFS 5037, and 2dFS 5038; and (viii) the giant NGC 346 1080. In Table 2, we have grouped these stars into the following three categories: OB supergiants, BA giants, and OB dwarfs. The formal uncertainties of their field measurements range from 60 to 1200 G and dipole field limits are between 1 and 12 kG. In the star VFTS 457, we obtained a field detection ($\langle B_z \rangle = 0.61 \pm 0.18$ kG) on the night of 19 February 2015, and the analysis of the full dataset provides moderate evidence that the star is magnetic (with an odds ratio of 11). The stellar spectrum is very close to the top edge of CHIP2, and part of the flux of the top beam falls into the gap between the two chips of the CCD, which impedes a correct spectrum extraction. The reliability of our detection is therefore highly questionable. In fact, the analysis of the null field values also provides moderate evidence that the star is magnetic, thus strongly supporting the hypothesis that our field detection is spurious. Therefore, the results for VFTS 457 have not been included in Table 2.

Some of our targets were observed with sufficient precision in order to detect typical magnetic fields observed in main sequence stars in the Galaxy. Recent results aimed at measuring magnetic fields in hot Galactic supergiants (e.g. Neiner et al. 2017; Martin et al. 2018) suggest that the fields in those objects are very weak, and it is therefore unsurprising to obtain non-detections in our survey.

5.3. Cool supergiants

The cool luminous supergiants [W60] D24, RM 1-546, and SkKM 179 were observed during our Of?p survey; the red supergiant VFTS 342 = WOH S 452 and the yellow supergiant CPD -69 463 were observed during our VMS survey. On the star TYC 8891-3239-1, which was observed during our run dedicated to Of?p stars, we formally detected a magnetic field during the night of 20/21 November 2017 ($\langle B_z \rangle = -55 \pm 15$ G). Another spectrum was obtained on 22/23 November 2017, but unfortunately it was saturated; therefore, detection could not be confirmed. We must point out that it is unlikely that an uncertainty of 15 G takes possible spurious effects due to small instrument flexures into account (Bagnulo et al. 2012); therefore, the star cannot be considered magnetic based only on one measurement. We also note that a 3σ detection is obtained from the analysis of the null field, further supporting the idea that the field detection is actually spurious. For all cool supergiants, the formal uncertainties (of the order of 50–125 G) are smaller than for our main targets, and they lead to low upper limits for the dipolar field (of the order of 1 kG, but as small as 175 G for [W60] D24). On the other hand, measurements of magnetic fields in cool giants and supergiants in the Milky Way (e.g. Grunhut et al. 2010) demonstrate that the surface magnetic fields of those stars have longitudinal components smaller than a few Gauss.

5.4. WR stars

The WR systems VFTS 457, VFTS 507, VFTS 509, VFTS 682, and R136c were observed in the 30 Dor region. No magnetic fields were formally detected with best formal uncertainties for individual stars ranging from 0.07–1 kG. For three WR stars,

our Bayesian analysis leads to upper limits of the dipolar field strength of the order of 1–3 kG. The VMS R136c was observed with a smaller precision leading to an upper limit of $B_{\text{dip}}^{(\text{max})} = 12.7 \text{ kG}$ for this star. As field measurements were carried out on emission lines, these estimates refer to the circumstellar environment rather than to the photospheric field.

5.5. Magnetic wind confinement of very massive stars

Seven of the observed stars are categorised as VMS: Mk37Wa, Mk42, R136c, VFTS 457, VFTS 506, VFTS 621, and VFTS 682. While the upper limits on the magnetic fields of these stars are all in the kG range, given the extremely powerful winds of these stars, it may still be possible that magnetic wind confinement can be ruled out. Since magnetic wind confinement can greatly reduce the net mass-loss rate and hence have a considerable impact on stellar evolution in the upper main sequence (e.g. [Petit et al. 2017](#)) and, therefore, on the mass of the final supernova product, it is of interest to determine whether this phenomenon is relevant to the VMS population.

We determined the magnetic wind confinement parameter η_* using Eq. (7) from [ud-Doula & Owocki \(2002\)](#), which also requires the stellar radius, mass-loss rate, and wind terminal velocity. The magnetic wind confinement parameter is simply the ratio of magnetic to kinetic energy density at the stellar surface. If η_* is greater than unity, the wind is magnetically confined. These parameters were obtained from [Bestenlehner et al. \(2014\)](#), where radii were determined from the effective temperatures and luminosities given by [Bestenlehner et al. \(2014\)](#).

We note that $\langle B_z \rangle$ measurements were conducted using emission lines for VFTS 457, 621, and 682; therefore, these measurements probe the circumstellar environment and cannot be used to constrain the photospheric magnetic field (Sect. 5.4; see also Table A.2). Since the calculation of η_* requires knowledge of the photospheric magnetic field strength, we excluded these three stars from this analysis. Of the remaining four stars, the spectra of Mk 37Wa and R136c are blended (Table A.2). However, we have made the assumption that the VMS component dominates the spectrum and that the correction to $\langle B_z \rangle$ for the presence of a second star is negligible.

The results are given in Table 3. The magnetic wind confinement parameter corresponding to $B_{\text{dip}}^{(\text{max})}$ in Table 2 (i.e. the 95% upper limit for B_{dip}) is given by η_*^{95} . In no case can a magnetically confined wind be ruled out at 95% confidence. However, the probability that η_* is below one is greater than 50% in all cases, and it is almost 85% for Mk 42.

The final column of Table 3 gives the value of the Alfvén radius R_A corresponding to η_*^{95} . The Alfvén radius is the distance from the star at which the wind opens the magnetic field lines; beyond R_A , the star no longer has a magnetosphere. We determined R_A by using the η_* dipole scaling given by [ud-Doula et al. \(2008; their Eq. \(9\)\)](#). In every case $R_A^{95} < 4R_*$, and in the case of Mk 42, it is $1.9 R_*$. It is therefore possible that the VMS may have magnetospheres of sizes comparable to those of the Galactic Of?p stars ([Petit et al. 2013](#)). Following [ud-Doula et al. \(2008; see also Petit et al. 2017\)](#), a reduction in the net mass-loss rate due to magnetic confinement of between about 40 and 80% cannot be ruled out.

In order to examine the wind confinement properties of the population of VMS, we constructed a global PDF by assuming each star contributes probabilistically to various values of η_* (as done by [David-Uraz et al. 2014](#), for the case of Galactic O-type stars). The resulting global PDF is shown in Fig. 8. The global

Table 3. Magnetic wind confinement parameters for Of?p and VMS targets.

Star	R_* (R_\odot)	$\log \dot{M}$ ($M_\odot \text{ yr}^{-1}$)	v_∞ (km s^{-1})	η_*^{95}	$P_{\eta_* < 1}$ (%)	R_A^{95} (R_*)
VMS						
Mk37Wa	31	−4.6	2530	141	58	3.7
Mk42	28	−3.9	2840	6	85	1.9
R136c	37	−3.9	1910	171	57	3.9
VFTS 506	20	−5.6	3040	60	73	3.1
Of?p						
AzV220	10.1	−6.5	2330	132	69	3.7
LMC164-2	8.4	−6.4	2330	206	61	4.1
SMC159-2	6.6	−6.8	1900	2987	44	7.7
LMCε136-1	7.5	−6.5	2170	330	58	4.6

Notes. η_*^{95} is the value of η_* corresponding to $B_{\text{dip}}^{(\text{max})}$ in Table 2, and R_A^{95} is the corresponding Alfvén radius. $P_{\eta_* < 1}$ is the probability that η_* is below one. The parameters used to determine η_* and R_* were obtained from [Bestenlehner et al. \(2014\)](#) for the VMS and from [Munoz et al. \(2020\)](#) for the Of?p stars.

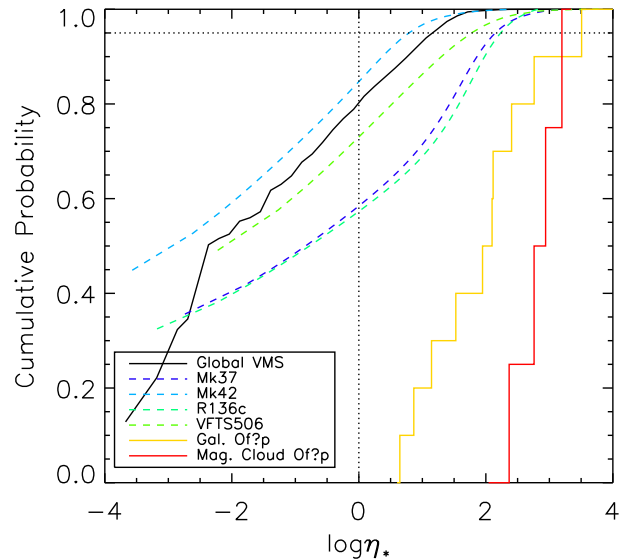


Fig. 8. Cumulative probabilities for η_* for individual VMS, Galactic, and extra-galactic Of?p stars (dashed curves), and the global probability for all VMS (solid curve). The vertical and horizontal dotted lines indicate $\eta_* = 1$ and the 95% confidence level, respectively.

PDF indicates that 80% of the population of VMS should have $\eta_* < 1$, that is, the winds of most of the members of this population are not magnetically confined. Also, 95% of the population should have $\eta_* < 14$.

For a comparison, we also determined the magnetic wind confinement parameters for the Of?p stars using the upper limits on B_{dip} determined for these stars. Here, we used the fundamental and stellar wind parameters determined for these stars by [Munoz et al. \(2020\)](#). The results are given in Table 3. The Of?p stars have, in general, lower probabilities of possessing magnetically unconfined winds, which is reassuring as the winds of these stars must be magnetically unconfined. Correspondingly, the upper limits on η_* and R_A are significantly higher than those

for the VMS. A further and more rigorous comparison is provided by examining the values of η_* for the Magellanic Cloud Of?p stars inferred by Munoz et al. (2020) via ADM modelling as well as the values of η_* for Galactic Of?p stars determined directly from magnetic measurements. For the Galactic stars, we used the values published by Petit et al. (2013), with the exception of updated values for ζ Ori Aa (Blazère et al. 2015) and HD 108 (Shultz & Wade 2017), and the value determined by Castro et al. (2015) for the magnetic O-type star HD 54879. The cumulative distributions of the $\log \eta_*$ values of Galactic and extra-galactic magnetic O-type stars are shown in Fig. 8. Both are clearly distinct from the VMS sample. In particular, all have η_* unambiguously greater than unity.

While the upper limits on η_* for the VMS cannot rule out magnetospheres that are comparable in extent to those of Galactic Of?p stars, it should be emphasised that VMS have not been reported to show the observational signatures of magnetic wind confinement and, in particular, rotational modulation of emission lines. There is, therefore, no evidence that magnetic fields play an important role in the circumstellar environments of these stars. We conclude that it is unlikely that these stars have magnetospheres.

6. Conclusions

We have obtained new magnetic field measurements of over 40 extra-galactic stars. Our main targets were Of?p stars and VMS, but we have also collected several measurements of stars in the vicinity of our main targets by taking advantage of the multi-object capabilities of the FORS2 instrument, which we employed for our observations. By adding up the data presented in this paper with those previously obtained by Bagnulo et al. (2017), we have collected 124 magnetic field measurements of 55 different extra-galactic stars in total. Our final list of observed targets includes five Of?p stars, seven VMS (five O supergiants and two WR stars), and various other giant, supergiant, and WR stars. None of our measurements may be considered as a definite detection, but the results of Bayesian statistical analysis strongly suggest that the Of?p star SMC 159-2 is magnetic, with a dipolar field strength probably of the order of a 2 to 4 kG. Our data show no evidence that any of the remaining known Of?p stars of the Magellanic Clouds are magnetic and set upper limits for their dipolar field strength of the order of 3–4 kG.

We estimated that for the VMS, the typical upper limit on the dipolar field strength is of the order of a few thousand Gauss. Our measurements are therefore unable to probe the regime (a few hundred Gauss) predicted by the magnetic spot model proposed by Cantiello & Braithwaite (2011). Our results do, however, suggest that not a large fraction of VMS have strong magnetic fields. In fact, the non-detection status is compatible with a magnetic incidence similar to that of Galactic OBA stars, or even lower values. This could be interpreted in three possible ways: either (i) VMS do not form via stellar mergers but, more likely, by classical disc fragmentation, or alternatively (ii) stellar mergers do not always result in the formation of strong magnetic fields, or (iii) the magnetic field decays more quickly in VMS than in canonical massive stars. New measurements of magnetic fields in VMS are needed to put tighter constraints on the possible dipolar strength of VMS, and constrain the formation of these important objects in the Universe.

In the evolved hot stars (luminosity class I and II), because of magnetic flux conservation, we expect very weak fields at the surface, much weaker than for MS stars (Neiner et al. 2017;

Keszthelyi et al. 2019). These fields are in fact very difficult to detect even on Galactic bright stars. Therefore, the fact that we did not detect fields in evolved stars is not surprising.

Acknowledgements. Based on observations made with ESO Telescopes at the La Silla Paranal Observatory under programme IDs 094.D-0533 and 0100.D-0670. We thank the referee Dr. McSwain for a very careful review and very useful comments. Y.N. acknowledges support from the Fonds National de la Recherche Scientifique (Belgium) and the University of Liège, as well as general support from the PRODEX XMM contract. G.A.W. acknowledges Discovery Grant support from the Natural Science and Engineering Research Council (NSERC) of Canada. A.D.U. gratefully acknowledges the support of NSERC. M.K.Sz. acknowledges support from the National Science Centre, Poland, grant MAESTRO 2014/14/A/ST9/00121. M.E.S. acknowledges the Annie Jump Cannon Fellowship, supported by the University of Delaware and endowed by the Mount Cuba Astronomical Observatory.

References

- Appenzeller, I., & Rupprecht, G. 1992, *The Messenger*, 67, 18
 Appenzeller, I., Fricke, K., Fürtig, W., et al. 1998, *The Messenger*, 94, 1
 Asensio Ramos, A., Martínez González, M. J., Manso Sainz, R., Corradi, R. L. M., & Leone, F. 2014, *ApJ*, 787, 111
 Augustson, K. C., Brun, A. S., & Toomre, J. 2016, *ApJ*, 829, 92
 Babcock, H. W. 1954, *ApJ*, 120, 66
 Babcock, H. W. 1958, *ApJS*, 3, 141
 Bagnulo, S., Szeifert, T., Wade, G. A., Landstreet, J. D., & Mathys, G. 2002, *A&A*, 389, 191
 Bagnulo, S., Landolfi, M., Landstreet, J. D., et al. 2009, *PASP*, 121, 993
 Bagnulo, S., Landstreet, J. D., Fossati, L., & Kochukhov, O. 2012, *A&A*, 538, A129
 Bagnulo, S., Fossati, L., Kochukhov, O., & Landstreet, J. D. 2013, *A&A*, 559, A103
 Bagnulo, S., Fossati, L., Landstreet, J. D., & Izzo, C. 2015, *A&A*, 583, A115
 Bagnulo, S., Nazé, Y., Howarth, I. D., et al. 2017, *A&A*, 601, A136
 Bestenlehner, J. M., Vink, J. S., Gräfener, G., et al. 2011, *A&A*, 530, L14
 Bestenlehner, J. M., Gräfener, G., Vink, J. S., et al. 2014, *A&A*, 570, A38
 Blazère, A., Neiner, C., Tkachenko, A., Bouret, J. C., & Rivinius, T. 2015, *A&A*, 582, A110
 Braithwaite, J., & Spruit, H. C. 2004, *Nature*, 431, 819
 Cantiello, M., & Braithwaite, J. 2011, *A&A*, 534, A140
 Cantiello, M., Langer, N., Brott, I., et al. 2009, *A&A*, 499, 279
 Casini, R., & Landi Degl'Innocenti, E. 1994, *A&A*, 291, 668
 Castro, N., Fossati, L., Hubrig, S., et al. 2015, *A&A*, 581, A81
 Crowther, P. A., Schnurr, O., Hirschi, R., et al. 2010, *MNRAS*, 408, 731
 David-Uraz, A., Wade, G. A., Petit, V., et al. 2014, *MNRAS*, 444, 429
 Donati, J.-F., & Landstreet, J. D. 2009, *ARA&A*, 47, 333
 Donati, J.-F., Semel, M., Carter, B. D., Rees, D. E., & Collier Cameron, A. 1997, *MNRAS*, 291, 658
 Driessen, F. A., Sundqvist, J. O., & Wade, G. A. 2018, ArXiv e-prints [arXiv:1811.00163]
 Evans, C. J., Taylor, W. D., Hénault-Brunet, V., et al. 2011, *A&A*, 530, A108
 Feitzinger, J. V., Schlosser, W., Schmidt-Kaler, T., & Winkler, C. 1980, *A&A*, 84, 50
 Ferrario, L., Pringle, J. E., Tout, C. A., & Wickramasinghe, D. T. 2009, *MNRAS*, 400, L71
 Fossati, L., Castro, N., Schöller, M., et al. 2015, *A&A*, 582, A45
 Georgy, C., Hirschi, R., & Ekström, S. 2017, in *Second BRITE-Constellation Science Conference: Small satellites-big science, Proceedings of the Polish Astronomical Society volume 5, held 22-26 August, 2016 in Innsbruck*, eds. K. Zwintz & E. Poretti, 18, 37
 Gregory, P. C. 2005, *Bayesian Logical Data Analysis for the Physical Sciences: A Comparative Approach with 'Mathematica' Support* (Cambridge: Cambridge University Press)
 Grunhut, J. H., Wade, G. A., Hanes, D. A., & Alecian, E. 2010, *MNRAS*, 408, 2290
 Grunhut, J. H., Wade, G. A., Sundqvist, J. O., et al. 2012, *MNRAS*, 426, 2208
 Grunhut, J. H., Wade, G. A., Neiner, C., et al. 2017, *MNRAS*, 465, 2432
 Keszthelyi, Z., Puls, J., & Wade, G. A. 2017, *A&A*, 598, A4
 Keszthelyi, Z., Meynet, G., Georgy, C., et al. 2019, *MNRAS*, 485, 5843
 Kolenberg, K., & Bagnulo, S. 2009, *A&A*, 498, 543
 Krumholz, M. R. 2015, *Very Massive Stars in the Local Universe* Astrophys. Space Sci. Lib., ed. J. S. Vink (Berlin: Springer), 412, 43

- Landstreet, J. D., & Mathys, G. 2000, *A&A*, **359**, 213
- Landstreet, J. D., Bagnulo, S., & Fossati, L. 2014, *A&A*, **572**, A113
- Martin, A. J., Neiner, C., Oksala, M. E., et al. 2018, *MNRAS*, **475**, 1521
- Massey, P., & Duffy, A. S. 2001, *ApJ*, **550**, 713
- Massey, P., Neugent, K. F., Morrell, N., & Hillier, D. J. 2014, *ApJ*, **788**, 83
- Melena, N. W., Massey, P., Morrell, N. I., & Zangari, A. M. 2008, *AJ*, **135**, 878
- Melnick, J. 1985, *A&A*, **153**, 235
- Mestel, L. 2001, *ASP Conf. Ser.*, **248**, 3
- Meynet, G., Eggenberger, P., & Maeder, A. 2011, *A&A*, **525**, L11
- Moffat, A. F. J., Poitras, V., Marchenko, S. V., et al. 2004, *AJ*, **128**, 2854
- Moss, D. 2001, *ASP Conf. Ser.*, **248**, 305
- Munoz, M. S., Wade, G. A., Nazé, Y., et al. 2020, *MNRAS*, **492**, 1199
- Nazé, Y., Petit, V., Rinbrand, M., et al. 2014, *ApJS*, **215**, 10
- Nazé, Y., Walborn, N. R., Morrell, N., Wade, G. A., & Szymański, M. K. 2015, *A&A*, **577**, A107
- Nazé, Y., Neiner, C., Grunhut, J., et al. 2017, *MNRAS*, **467**, 501
- Neiner, C., Mathis, S., Alecian, E., et al. 2015a, *IAU Symp.*, **305**, 61
- Neiner, C., Grunhut, J., Leroy, B., De Becker, M., & Rauw, G. 2015b, *A&A*, **575**, A66
- Neiner, C., Oksala, M. E., Georgy, C., et al. 2017, *MNRAS*, **471**, 1926
- Neugent, K. F., Massey, P., Skiff, B., & Meynet, G. 2012, *AJ*, **749**, 177
- Neugent, K. F., Massey, P., & Morrell, N. 2018, *ApJ*, **863**, 181
- Oksala, M. E., Wade, G. A., Townsend, R. H. D., et al. 2012, *MNRAS*, **419**, 959
- Owocki, S. P., ud-Doula, A., Sundqvist, J. O., et al. 2016, *MNRAS*, **462**, 3830
- Petit, V., & Wade, G. A. 2012, *MNRAS*, **420**, 773
- Petit, V., Owocki, S. P., Wade, G. A., et al. 2013, *MNRAS*, **429**, 398
- Petit, V., Keszthelyi, Z., MacInnis, R., et al. 2017, *MNRAS*, **466**, 1052
- Petit, V., Wade, G. A., Schneider, F. R. N., et al. 2019, *MNRAS*, **489**, 5669
- Reiners, A. 2012, *Liv. Rev. Sol. Phys.*, **9**, 1
- Sabín-Sanjulián, C., Simón-Díaz, S., Herrero, A., et al. 2014, *A&A*, **564**, A39
- Schneider, F. R. N., Podsiadlowski, P., Langer, N., Castro, N., & Fossati, L. 2016, *MNRAS*, **457**, 2355
- Schneider, F. R. N., Ohlmann, S. T., Podsiadlowski, P., et al. 2019, *Nature*, **574**, 211
- Schnurr, O., Chené, A. N., Casoli, J., Moffat, A. F. J., & St-Louis, N. 2009, *MNRAS*, **397**, 2049
- Shultz, M., & Wade, G. A. 2017, *MNRAS*, **468**, 3985
- Shultz, M., Wade, G. A., Alecian, E., & BinaMiCS Collaboration 2015, *MNRAS*, **454**, L1
- Shultz, M. E., Wade, G. A., Rivinius, T., et al. 2018, *MNRAS*, **475**, 5144
- Shultz, M. E., Wade, G. A., Rivinius, T., et al. 2019, *MNRAS*, **490**, 274
- Sikora, J., Wade, G. A., Power, J., & Neiner, C. 2019a, *MNRAS*, **483**, 2300
- Sikora, J., Wade, G. A., Power, J., & Neiner, C. 2019b, *MNRAS*, **483**, 3127
- Tout, C. A., Wickramasinghe, D. T., Liebert, J., Ferrario, L., & Pringle, J. E. 2008, *MNRAS*, **387**, 897
- Townsend, R. H. D., Oksala, M. E., Cohen, D. H., Owocki, S. P., & ud-Doula, A. 2010, *ApJ*, **714**, L318
- Tutukov, A. V., & Fedorova, A. V. 2010, *Astron. Rep.*, **54**, 156
- ud-Doula, A., & Owocki, S. P. 2002, *ApJ*, **576**, 413
- ud-Doula, A., Owocki, S. P., & Townsend, R. H. D. 2008, *MNRAS*, **385**, 97
- ud-Doula, A., Owocki, S. P., & Townsend, R. H. D. 2009, *MNRAS*, **392**, 1022
- ud-Doula, A., Sundqvist, J. O., Owocki, S. P., Petit, V., & Townsend, R. H. D. 2013, *MNRAS*, **428**, 2723
- Udalski, A., Szymański, M. K., & Szymański, G. 2015, *Acta Astron.*, **65**, 1
- Wade, G. A., Neiner, C., Alecian, E., et al. 2016, *MNRAS*, **456**, 2
- Walborn, N. R. 1972, *AJ*, **77**, 312
- Walborn, N. R. 1973, *AJ*, **78**, 1067
- Walborn, N. R., & Blades, J. C. 1987, *ApJ*, **323**, L65
- Walborn, N. R., Lennon, D. J., Heap, S. R., et al. 2000, *PASP*, **112**, 1243
- Walborn, N. R., Morrell, N. I., Nazé, Y., et al. 2015, *AJ*, **150**, 99
- Yusof, N., Hirschi, R., Meynet, G., et al. 2013, *MNRAS*, **433**, 1114

Appendix A: Observing log and magnetic field measurements

Table A.1. Log of the FORS2 observations obtained with grism 1200B in spectropolarimetric mode during the run dedicated to Of?p stars (listed in boldface fonts).

DATE	UT	RA	Dec	STAR	V	Sp.	Exp	S/N	$\langle B_z \rangle$	$\langle N_z \rangle$
yyyy-dd-mm	hh:mm	J2000						\AA^{-1}	G	G
2017-11-21	00:00	19:53:18.7	-03:06:52	HD 188041	5.6	F0 Vp	80	4090	772 ± 18	4 ± 9
2017-11-21	23:54						80	2765	779 ± 21	-21 ± 13
2017-11-21	08:50	10:55:01.0	-42:15:04	HD 94660	6.1	Ap	60	3010	-2345 ± 25	-15 ± 10
2017-11-22	01:28	00:49:47.6	-73:17:53	AzV 55	13.4	B5	6800	1480	-130 ± 60	5 ± 60
2017-11-24	02:25						8880	1610	-75 ± 60	-155 ± 60
2017-11-21	00:32	00:49:58.7	-73:19:28	SMC 159-2	15.1	O8f?p	7200	580	625 ± 405	-275 ± 425
2017-11-21	04:00						6400	540	580 ± 505	390 ± 485
2017-11-22	01:28						6800	605	1050 ± 430	865 ± 425
2017-11-24	02:25						8880	590	615 ± 420	1215 ± 440
2017-11-22	01:28	00:49:59.7	-73:18:42	2MASS J00495968-7 318 420	15.2	HPMS	6800	675	-185 ± 145	-35 ± 145
2017-11-24	02:25						8880	740	-325 ± 170	-95 ± 160
2017-11-22	01:28	00:50:04.8	-73:21:03	2dFS 5037	15.0	B0.5 (V)	6800	635	330 ± 260	-540 ± 265
2017-11-22	01:28	00:50:06.3	-73:16:32	AzV 66	13.5	B0.5 V	6800	1380	-75 ± 100	55 ± 100
2017-11-24	02:25						8880	1495	-215 ± 95	-285 ± 100
2017-11-22	01:28	00:50:17.5	-73:17:18	2dFS 5038	15.1	B0.5 (V)	6800	715	220 ± 190	-55 ± 195
2017-11-24	04:51	00:58:53.3	-72:08:35	SkKM 179	12.9	G8Iab-Ib	8800	850	-130 ± 50	-15 ± 50
2017-11-24	04:51	00:59:00.9	-72:07:18	NGC 346 ELS 27	15.0	B0.5 V	8800	550	-1005 ± 445	-130 ± 460
2017-11-24	04:51	00:59:04.2	-72:04:49	NGC 346 ELS 68	15.9	B0 V(Be-Fe)	8800	480	-675 ± 830	200 ± 920
2017-11-24	04:51	00:59:05.6	-72:08:02	NGC 346 ELS 19	14.9	A0 II	8800	525	-615 ± 315	685 ± 385
2017-11-24	04:51	00:59:10.0	-72:05:49	AzV 220	14.5	O6.5f?p	8800	845	-225 ± 305	-155 ± 290
2017-11-24	04:51	00:59:18.3	-72:04:21	NGC 346 1080	16.1	B0.5 III	8800	535	475 ± 395	575 ± 425
2017-11-24	04:51	00:59:20.8	-72:02:59	NGC 346 ELS 103	16.2	B0.5 V	8800	430	-320 ± 480	630 ± 490
2017-11-24	04:51	00:59:20.8	-72:03:38	NGC 346 ELS 100	16.1	B1.5 V	8800	430	-50 ± 595	190 ± 575
2017-11-21	06:40	05:31:09.9	-67:11:19	[W60] D24	13.2	M1 I	9600	1065	5 ± 30	-30 ± 30
2017-11-23	07:39						7200	1050	5 ± 30	15 ± 30
2017-11-21	06:40	05:31:54.5	-67:08:22	RM 1-546	13.4	M: E	9600	695	10 ± 50	70 ± 50
2017-11-23	07:39						7200	655	100 ± 45	-85 ± 50
2017-11-21	06:40	05:31:54.8	-67:11:21	2MASS 05315473-6711 194	14.7		9600	845	-395 ± 200	225 ± 205
2017-11-23	07:39						7200	820	-220 ± 200	350 ± 205
2017-11-21	06:40	05:32:22.9	-67:10:19	LMCe 136-1	14.6	O6.5f?p	9600	995	450 ± 235	-10 ± 235
2017-11-23	07:39						7200	890	-85 ± 275	-230 ± 280
2017-11-21	06:40	05:32:32.9	-67:10:42	TYC 8891-3239-1	11.3		9600	3085	-55 ± 15	-45 ± 15
2017-11-21	06:40	05:32:39.2	-67:09:49	2MASS 05323916-6709 487	14.4		9600	1095	375 ± 110	-25 ± 110
2017-11-23	07:39						7200	1060	130 ± 105	135 ± 105
2017-11-21	06:40	05:32:47.4	-67:10:05	SK-67 180	12.6	B3: I	9600	2280	-5 ± 50	30 ± 50
2017-11-23	07:39						7200	2260	-125 ± 55	85 ± 50
2017-11-21	06:40	05:32:55.2	-67:10:20	2MASS 05325508-6710 200	15.7	??	9600	580	-180 ± 325	-535 ± 325
2017-11-23	07:39						7200	575	320 ± 180	20 ± 280

Notes. The first two entries refer to known magnetic Ap stars. Columns 1 and 2 give the civilian date and UT time of the midpoint of the observation; Cols. 3–5 give the J2000 RA and Dec and the target name as identified through SIMBAD or other catalogues; Col. 6 gives the V magnitude; Col. 7 is the star's spectral type; Cols. 8 and 9 give the total exposure time and the S/N per \AA ; and Cols. 10 and 11 give our field determination from the reduced Stokes V profiles, $\langle B_z \rangle$, and from the null profiles, $\langle N_z \rangle$, respectively.

Table A.2. Log of the FORS2 observations from the run on very massive stars (VMS) and field measurements from absorption lines.

DATE	UT	RA	Dec	STAR	V	Sp. type	S/N	$\langle B_z \rangle$	$\langle N_z \rangle$	Note
yyyy-dd-mm	hh:mm	J2000					\AA^{-1}	G	G	
2015-03-05	01:37	05:38:17.7	-69:03:39	VFTS 291	14.9	B5 II-Ib	395	-75 ± 770	1035 ± 765	
2015-03-05	03:01			[HBC93] 275			355	910 ± 980	-815 ± 1005	
2015-02-19	03:38	05:38:26.7	-69:08:53	VFTS 341	14.0	K5Ia-Iab	560	105 ± 145	200 ± 150	
2015-02-25	03:14			WOH S 452			570	-185 ± 125	-20 ± 130	
2015-03-05	01:37						540	390 ± 145	30 ± 135	
2015-03-05	03:01						490	60 ± 170	210 ± 175	
2015-04-01	00:51						545	135 ± 130	-75 ± 145	
2015-02-19	03:38	05:38:37.8	-69:03:29	VFTS 441	15.1	O9.5V	340	-1660 ± 1025	-840 ± 960	
2015-02-25	03:14			[P93] 613			360	405 ± 1110	-900 ± 1100	
2015-04-01	00:51						375	-585 ± 1140	-555 ± 1110	
2015-02-19	03:38	05:38:38.8	-69:06:50	VFTS 457	13.7	O3.5 If*/WN7	645	605 ± 175	40 ± 100	1
2015-02-25	03:14			Mk 51			640	20 ± 140	445 ± 140	
2015-03-05	01:37						710	-600 ± 310	590 ± 285	
2015-03-05	03:01						620	-795 ± 340	780 ± 280	
2015-04-01	00:51						630	190 ± 140	-65 ± 135	
2015-03-05	01:37	05:38:38.9	-69:08:15	VFTS 458	12.6	BN6Iap	995	165 ± 285	-180 ± 260	
2015-03-05	03:01			HTR 13			895	-350 ± 360	645 ± 360	
2015-03-05	01:37	05:38:41.2	-69:02:58	VFTS 500	14.2	O6.5IV((fc))+O6.5V((fc))	590	790 ± 650	1390 ± 575	
2015-03-05	03:01			LMC 171 520			515	970 ± 655	-1880 ± 640	
2015-02-19	03:38	05:38:41.5	-69:05:20	VFTS 506	13.1	ON2V((n))((f*))	750	-50 ± 720	825 ± 690	
2015-02-25	03:14			NGC 2070 Mk 25			790	340 ± 705	-915 ± 695	
2015-04-01	00:51						795	-450 ± 670	225 ± 620	
2015-03-05	01:37	05:38:41.6	-69:05:13	VFTS 507	12.5	WC4+WN6+O	2220	125 ± 165	-260 ± 190	1,2
2015-03-05	03:01			R140a			2245	30 ± 160	-85 ± 155	
2015-03-05	01:37	05:38:41.6	-69:05:14	VFTS 509	12.8	WN6+O	1120	-60 ± 210	70 ± 180	1,2
2015-03-05	03:01			R140b			880	20 ± 300	-430 ± 270	
2015-02-19	03:38	05:38:41.9	-69:06:13	Mk 37Wa	14.9	O4If+	845	285 ± 735	-905 ± 685	2
2015-02-25	03:14			VFTS 1021			860	-1385 ± 640	1320 ± 580	
2015-04-01	00:51						910	-730 ± 545	760 ± 505	
2015-03-05	01:37	05:38:42.1	-69:05:55	Mk 42	11.0	O2If*	1175	-645 ± 430	195 ± 360	
2015-03-05	03:01			BAT99 105			1075	-220 ± 465	-135 ± 395	
2015-02-19	03:38	05:38:42.2	-69:08:32	VFTS 526	15.2	O8.5I((n))fp	350	-1195 ± 425	-530 ± 425	
2015-02-25	03:14			[P93] 925			350	-1055 ± 470	-1155 ± 480	
2015-04-01	00:51						340	-330 ± 505	-85 ± 425	
2015-02-19	03:38	05:38:42.7	-69:06:04	R136c		WN5h	1440	1065 ± 1290	-1030 ± 1120	2
2015-02-25	03:14			VFTS 1025			1200	1230 ± 1145	-100 ± 1110	
2015-04-01	00:51						1275	2745 ± 1300	-1480 ± 1300	
2015-02-19	03:38	05:38:45.4	-69:02:51	VFTS 586	14.5	O4V((n))((fc))z	370	1485 ± 1085	1645 ± 1020	
2015-02-25	03:14						365	-820 ± 690	-965 ± 775	
2015-04-01	00:51						375	1205 ± 845	1175 ± 870	
2015-03-05	01:37	05:38:45.6	-68:07:35	VFTS 589	15.8	B0.5V(SB2?)	270	1585 ± 1205	255 ± 1110	
2015-03-05	03:01			[P93] 1247			210	745 ± 1785	2185 ± 1775	
2015-02-19	03:38	05:38:48.1	-69:04:42	VFTS 621	15.4	O2V((f*))z	415	70 ± 285	-35 ± 195	1
2015-02-25	03:14			Walborn 2			465	-405 ± 330	-420 ± 365	
2015-04-01	00:51						525	-100 ± 700	100 ± 515	
2015-02-19	03:38	05:38:51.6	-69:08:07	CPD-69 463	12.0	F7Ia	1535	-170 ± 185	-55 ± 170	
2015-02-25	03:14			R143			1570	125 ± 155	180 ± 160	
2015-04-01	00:51						1540	-265 ± 180	-10 ± 185	
2015-03-05	01:37	05:38:55.5	-69:04:27	VFTS 682	16.1	WN5h	230	-30 ± 650	145 ± 665	1
2015-03-05	03:01			LMCe 1415			200	185 ± 755	-160 ± 770	1

Notes. Columns as in Table A.1, except that exposure time is not reported as it was identical (3296 s) for all observations. Column 5 gives two designations of the same target. Column 11 refers to the comments at the end of the Table. VMS names are typed with boldface fonts. (1) Magnetic field was estimated from emission lines. (2) Spectrum blended.